Materials Research Letters

ISSN: (Print) 2166-3831 (Online) Journal homepage: https://www.tandfonline.com/loi/tmrl20

Predicting band offset of lattice matched ZnO and BeCdO heterojunction from first principles

Xiaojie Liu, Junli Chen, Hang Yin, Lina Bai, Chengbao Yao, Hua Li, Haitao Yin & Yin Wang

To cite this article: Xiaojie Liu, Junli Chen, Hang Yin, Lina Bai, Chengbao Yao, Hua Li, Haitao Yin & Yin Wang (2019) Predicting band offset of lattice matched ZnO and BeCdO heterojunction from first principles, Materials Research Letters, 7:6, 232-238, DOI: 10.1080/21663831.2019.1593253

To link to this article: https://doi.org/10.1080/21663831.2019.1593253

MATER. RES. LETT.
2019, VOL. 7, NO. 6, 232–238
https://doi.org/10.1080/21663831.2019.1593253

MATERIALS RESEARCH LETTERS
Taylor & Francis
Taylor & Francis Group

ORIGINAL REPORT

Predicting band offset of lattice matched ZnO and BeCdO heterojunction from first principles

Xiaojie Liu[a], Junli Chen[a], Hang Yin[b], Lina Bai[a], Chengbao Yao[a], Hua Li[a], Haitao Yin[a,c] and Yin Wang [c,d]

[a]Key Laboratory for Photonic and Electronic Bandgap Materials of Ministry of Education, School of Physics and Electronic Engineering, Harbin Normal University, Harbin, People's Republic of China; [b]School of Electronics and Information Engineering, Harbin Institute of Technology, Harbin, People's Republic of China; [c]Department of Physics and the Center of Theoretical and Computational Physics, The University of Hong Kong, Hong Kong SAR, People's Republic of China; [d]Department of Physics and International Centre for Quantum and Molecular Structures, Shanghai University, Shanghai, People's Republic of China

ABSTRACT

Using first-principles approach, we calculated the band gaps of *wurtzite* $Be_{1-x}Cd_xO$ ternary alloy and the band offset of the *lattice matched* $ZnO/Be_{0.44}Cd_{0.56}O[1\,1\,\bar{2}\,0]$ heterojunction, where the modified Becke–Johnson semi-local exchange was used to determine the band gap and the coherent potential approximation was applied to deal with doping effect in disordered alloys. The $ZnO/Be_{0.44}Cd_{0.56}O$ heterojunction was determined to have a type II band alignment, with valence and conduction band offset being 0.28 and 0.50 eV, respectively. The calculation approach and procedure demonstrated here can be used to predict the band offset of more *lattice matched* semiconductor heterojunctions.

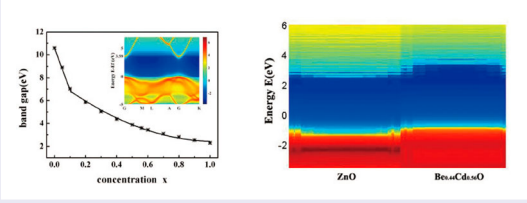

IMPACT STATEMENT

The band offsets of *lattice matched* $ZnO/Be_{0.44}Cd_{0.56}O$ heterojunction were predicted from first principles, where band gaps of semiconductors and configuration average of disorders were both accurately and efficiently calculated.

ARTICLE HISTORY
Received 14 March 2018

KEYWORDS
Band offset; band gap; heterojunction; first principles; semiconductor alloy

1. Introduction

For the design of electronic devices, the band alignment of heterostructure plays a vital role as the distribution of carriers determine the optical characteristics of the device [1,2]. If a semiconductor heterojunction A/B that formed by two different semiconductor compounds A and B has a type I band alignment, both electrons and holes are confined in the narrower band gap semiconductor and may recombine with each other more efficiently. Such heterojunctions are commonly used in LEDs or laser diodes. For instance, in ZnO-based semiconductor technology $Zn_{1-x}Mg_xO$ ternary alloy [3,4] which has a wider band gap than that of pure ZnO is usually considered as one of the barrier materials for forming type I semiconductor heterojunction $ZnO/Zn_{1-x}Mg_xO$ [5,6].

Zinc oxide (ZnO), with a direct band gap of 3.37 eV and a higher exciton binding energy of about 60 meV at room temperature [7–9], is a popular and promising material in the field of photovoltaic devices and optoelectronics, such as solar cells [10], light-emitting diodes (LEDs) [11], nano-scale ultraviolet lasers [12]. However, for these photovoltaic devices, the charge

CONTACT Haitao Yin wlyht@126.com Key Laboratory for Photonic and Electronic Bandgap Materials of Ministry of Education, School of Physics and Electronic Engineering, Harbin Normal University, Harbin 150025, People's Republic of China; Department of Physics and the Center of Theoretical and Computational Physics, The University of Hong Kong, Pokfulam Road, Hong Kong SAR, People's Republic of China; Yin Wang yinwang@shu.edu.cn Department of Physics and the Center of Theoretical and Computational Physics, The University of Hong Kong, Pokfulam Road, Hong Kong SAR, People's Republic of China; Department of Physics and International Centre for Quantum and Molecular Structures, Shanghai University, 99 Shangda Road, Shanghai 200444, People's Republic of China

separation of the electron and hole is a key step in the generation of solar power. In nanometer architecture photovoltaic device, the charge separation is often facilitated by a heterojunction A/B with type II band alignment. For instance, in ZnO-based semiconductor technology, ZnO/ZnSe [13], ZnO/ZnS [14], ZnO/CdTe [15], $ZnO/ZnFe_2O_4$ [16] heterojunctions are all determined to have type II band alignment and have been intensively investigated for solar cell applications. However, the lattice mismatch ratios in the above heterostructures are larger than 18%, and such a big lattice mismatch ratio, in principle, induces larger crystal mosaics [17,18], higher residual carrier concentration [19], and threading dislocations [20], which greatly hinder the optical performance of the photovoltaic devices. It is therefore very important to grow *lattice matched* heterostructures, and doping one part or both parts of the heterostructure is an effective way.

Considering that the lattice constant of a semiconductor can be simply adjusted by doping, it is clearly possible to form *lattice matched* heterojunction using pure ZnO and a ternary semiconductor alloy. Because the concentration of each composition is both sensitive to the lattice constant of the semiconductor alloy and the band alignment of the heterojunction, it is therefore very important and useful to develop a theoretical method which can predict the band alignment between semiconductor alloys, so that the composition of the semiconductor species and the corresponding concentration can be determined in advance to avoid costly and tedious experimental explorations. First-principles approaches are obviously the most promising method to make these predictions, whereas, the calculations of the band offset of semiconductor alloys from first principles have always been a serious challenge [21–24]. Firstly, the traditional first-principles methods usually underestimate the band gap of semiconductors within a reasonable calculation cost, resulting in the failure to predict the conduction band offset of the heterojunction. Some advanced methods such as GW [25] and hybrid functional [26] can yield correct band gap but require huge calculation cost which are hard to calculate heterojunctions involving around hundred atoms or more. Next, the calculations of semiconductor with impurities [27] also increase the calculation cost, especially when the concentration of one species is very small, because one needs to compute systems with a large number of host atoms to accommodate the impurities and to take configuration average over many calculations to obtain a more reliable physical result. Thirdly, transport property is crucial for heterojunction and related devices. One of the most widely used and standard methods to calculate the transport properties of mesoscopic systems from first principles is the so-called NEGF-DFT method which combines the non-equilibrium Green's function (NEGF) and density functional theory (DFT) to deal with the non-equilibrium statistics [28,29]. To calculate using NEGF-DFT method, only localized basis sets such as LMTO and linear combination of atomic orbitals (LCAO) are suitable, because plane-wave basis set will generate dense matrix which needs huge time to inverse when constructing the Green's function. To overcome the calculation challenges and further study the transport properties, we have proposed a theoretical method to calculate the composition dependent band offset of semiconductor heterojunctions [5,30], which uses modified Becke–Johnson (MBJ) semi-local exchange functional [31] to obtain accurate band gaps for semiconductors within reasonable calculation cost [32] and the coherent potential approximation (CPA) [33] to deal with the doping effect for semiconductor alloys and to overcome the prohibitively large computation required for performing configuration average. Previously, the method has been used to calculate the composition dependent band gaps and band offsets for group III–V [30,34], group IV [35], group II–VI [5] semiconductor alloys and their heterojunctions, and quantitative comparisons to the existing experimental data are made.

In this work, we carried out first-principles calculations within the CPA-MBJ approach to predict the band alignment of $ZnO/Be_{1-x}Cd_xO$ ($x = 0.56$) heterojunction, where the $Be_{1-x}Cd_xO$ alloy and ZnO have matched lattice constant. It is well accepted that the theoretical predictions are of great fundamental interest as well as practical relevance. In particular, as nanoelectronic devices are reaching the sub-10 nm scale, atomistic first-principle prediction of band parameters of semiconductor heterostructures is becoming very important to design of new device architecture and select of new electronic materials that have desired properties for the next generation devices. The rest of the paper is organized as follows. In the next section, the calculation method and details are briefly discussed. Section 3 presents the results and Section 4 is a short summary.

2. Calculation methods and details

Our first-principles calculations are based on density functional theory (DFT), where the linear muffin-tin orbital (LMTO) is used with the atomic sphere approximation (ASA) [36], as implemented in Nanodsim software package [37]. In our calculations, the primitive cell of the *wurtzite* structure was used to calculate the band structures and band gaps (E_g) of the semiconductor compounds. The lattice constants of these pure hexagonal *wurtzite* structures are adopted from Refs. [38–40] and

Table 1. Lattice parameters for *wurtzite* ZnO, BeO and CdO crystals.

Crystal	a (Å)	c (Å)	u
ZnO [38]	3.2495	5.2069	0.382
BeO [39]	2.718	4.409	0.378
CdO [40]	3.660	5.856	0.350

are listed in Table 1. For the ternary alloy $Be_{1-x}Cd_xO$, the lattice constants are determined by the Vegard law [41] as

$$a_{BeCdO}(x) = xa_{CdO} + (1-x)a_{BeO}, \quad (1)$$

$$c_{BeCdO}(x) = xc_{CdO} + (1-x)c_{BeO}, \quad (2)$$

where x is the concentration Cd in Cd-doped *wurtzite* BeO. To calculate the band offset of ZnO and the ternary alloy, ZnO/BeCdO heterojunction with the lattice constant of pure ZnO is used to determine the potential profile across the interface. Clearly, the lattice constant of the $Be_{0.44}Cd_{0.56}O$ ternary alloy equals to the lattice constant of the pure ZnO according to the Vegard law. Although CdO usually forms *rock-salt* structure, the *wurtzite* CdO is calculated to be an additional local minimum, and the total energy of both CdO structures are the same within the precision of the first-principles calculations [40]. Moreover, experiments also show that CdO can form *wurtzite* ternary alloys in a wide range of CdO concentration from 0 to 69% [42]. Therefore, in all the calculations of this work, we only consider *wurtzite* structure for the studied semiconductors.

For ASA, empty spheres were placed at appropriate locations for space filling. The *wurtzite* structure can be made nearly close packed by adding two types of vacancy sites [Figure 1(d)]. For technical details of the atomic sphere positions and radii, we refer interested readers to Ref. [34]. The MBJ semi-local exchange functional is used to accurately determine the band gap of semiconductors. Following the original paper [31], the MBJ semi-local exchange potential has the following form:

$$v_{x,\sigma}^{MBJ}(r) = c' v_{x,\sigma}^{BR}(r) + (3c'-2)\frac{1}{\pi}\sqrt{\frac{5}{12}}\sqrt{\frac{2t_\sigma(r)}{\rho_\sigma(r)}}, \quad (3)$$

where subscript σ denotes spin, and ρ_σ the electron density for spin channel σ. The quantity t_σ is the kinetic energy density, and $v_{x,\sigma}^{BR}(r)$ the Becke–Roussel potential. The above MBJ potential has two terms whose relative weight is given by a parameter c'. It was shown in Ref. [31] that the value of c' depends linearly on the square root of the average of $\nabla\rho/\rho$. The parameter c' can be determined self-consistently as discussed in Refs. [31,43]. In our calculations the c' values are 'local', namely, different c' values are used for different real atom and vacancy

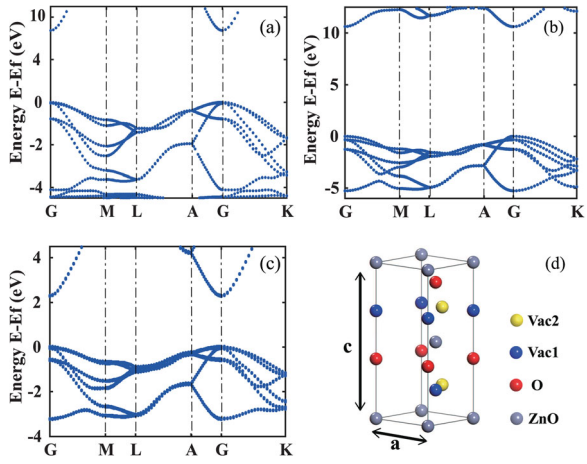

Figure 1. (Color online) Band structure for *wurtzite* (a) ZnO, (b) BeO, and (c) CdO with the calculated band gap of 3.37, 10.60 and 2.30 eV, respectively. (d) The real atoms and vacancy spheres for the ASA of the *wurtzite* ZnO, gray, red, blue and yellow balls show Zn, O, and two different vacancy spheres to fill the space for ASA, respectively.

spheres in ASA, and these values are pre-determined by fitting the accurate band gap of pure ZnO and BeO [44]. The c' parameter of Cd is the same as that of Be. During the self-consistent iterations, Zn and Cd *3d* electrons are treated as valence electrons. The band gap of semiconductor alloy can be obtained from the spectral function calculations. To more intuitively read the band gap information, we plot the spectral function as a function of both momentum k and energy E as

$$D(E,k) \equiv -\frac{1}{\pi} ImTr\overline{G^r(E,k)}, \quad (4)$$

where $\overline{G^r(E,k)}$ is the disorder average of retarded Green's function, which can be carried out analytically in disordered bulk materials. In this way, the spectral function can trace like the band structure of the pure semiconductor as shown in the following section.

3. Results and discussions

The calculated band structures of *wurtzite* ZnO, BeO and CdO with band gap of 3.37, 10.60 and 2.30 eV, respectively, are shown in Figure 1. Compared with the band gaps from the local density approximation (LDA), and generalized gradient approximation (GGA), the opening of band gap is evident as listed in the Table 2, and our calculated MBJ band gaps are in good agreement with the existing experimental values. Furthermore, using the LMTO–CPA–MBJ method, we calculated band gap across the entire concentration range for *wurtzite* $Be_{1-x}Cd_xO$ alloy as plotted in Figure 2. Note that when BeO crystal is doped with impurity atoms

Table 2. Theoretical and experimental fundamental band gaps of ZnO, BeO and CdO (in the unit of eV).

Crystal	LDA	GGA	MBJ	Expt.
ZnO	0.73 [45]	0.77 [46]	3.37	3.37 [7]
BeO	7.36 [47]	7.66 [48]	10.60	10.60 [49]
CdO	0.9* [50]	0.00083 [51]	2.30	–

Notes: Note that the band gap value of CdO indicated by the star sign was obtained from the LDA+U method. MBJ values were calculated in this work. We note that the parameter c' is tuned to make the MBJ calculated band gaps match the experimental values.

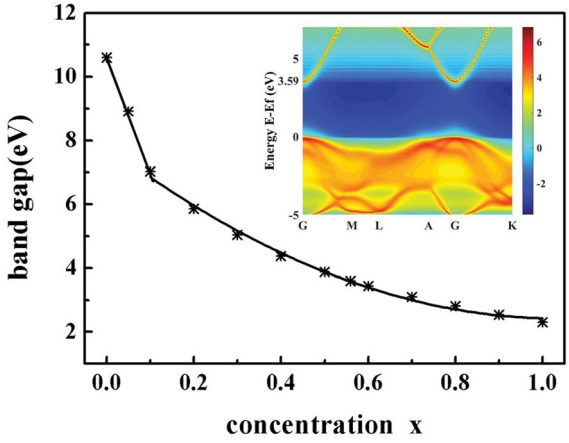

Figure 2. (Color online) Band gap of $Be_{1-x}Cd_xO$ versus x for *wurtzite* crystal structure by the MBJ-CPA approach. Black stars: the calculated data, solid lines: the fitted curve. Inset: the calculated spectral function for the $Be_{0.44}Cd_{0.56}O$ alloy in logarithmic scale as a function of momentum k and energy E with the band gap of 3.59 eV.

at random sites, translational symmetry is broken and momentum k is no-longer a good quantum number such that Bloch's theorem no longer exists. With including CPA in calculations, we can construct an effective medium by completing configurational average over the random disorder that restores the translational invariance. Our results show that the band gap of $Be_{1-x}Cd_xO$ continuously decreases from 10.60 to 2.30 eV as x is increased from 0 to 1. As x increases, $E_g(x)$ drops sharply when $x < 0.1$, then decreases slower when $x > 0.1$. By fitting the calculated results, we obtained that the band gaps of the $Be_{1-x}Cd_xO$ alloys scale as a linear function of $E_g = 10.63 - -35.68x$ at low impurity concentration $x < 0.1$ and a quadratic function of $E_g = 7.45 - -9.11x + 4.03x^2$ when $x > 0.1$ as shown by the solid lines in Figure 2. The reduction of band gap can be attributed to the contributions of the hybridization of Be-*2s* and Cd-*5s*, the enhancement of *p*-*d* repulsion: the valence band maximum of the alloy is contributed from O-*2p* electrons and the conduction band minimum is from Cd-*5s* and Be-*2s* states. With the increasing of Cd concentration in $Be_{1-x}Cd_xO$ alloy, the repulsion effect between Cd-*4d* and O-*2p* is enhanced and, therefore, the valence band maximum is risen. The energy of the Cd-*5s* is less than the energy of Be-*2s*, therefore, doping Cd in BeO will significantly reduce the conduction band minimum [51]. Moreover, from the inset of Figure 2, we can read that the band gap of the $Be_{0.44}Cd_{0.56}O$ alloy is 3.59 eV, which is much lower than that of the pure BeO of 10.60 eV. Our calculated gap of $Be_{0.44}Cd_{0.56}O$ (3.59 eV) agrees reasonably well with the results of Ref. [51], where they calculated the band gap of BeCdO alloy with the scissors-corrected GGA method.

Having correctly determined the band gaps of ZnO and $Be_{0.44}Cd_{0.56}O$ alloy, we further calculated the band offsets of the *lattice matched* ZnO/$Be_{0.44}Cd_{0.56}O$ heterojunction. The valence band offset (VBO) and conduction band offset (CBO) of a heterojunction are defined as the difference between the energy values of the top of the valence bands and the bottom of the conduction bands of the two semiconductors forming the junction, respectively. To calculate the band offsets, we consider the heterojunction A/B which is formed by two *lattice matched* semiconductors A and B. In an individual calculation for each semiconductor A or B, the valence band edge $E_v(A)$ or $E_v(B)$ can be obtained with respect to the average of the electrostatic potential $E_{es}(A)$ or $E_{es}(B)$ in each bulk material. However, because the calculations on the two materials A and B are carried out independently, namely, the energies in A or B are not referred to the same reference point in energy, the energy relation between the two calculations are ill-defined. Therefore, the manipulation of adding or subtracting energies between A and B is of no any physical meaning.

To calculate the band offset of heterojunction A/B, we further carried out a calculation on the heterojunction A/B where each part A and B are long enough so that the electrostatic potential $E_{es}(A)'$ or $E_{es}(B)'$ in the center regions of both A and B are not affected by the interface. Because the energies in A or B in the heterojunction are referred to the same reference point in the calculation, we can obtain the valence band offset (VBO) from the difference between the valence band edge $E_v(A)'$ and $E_v(B)'$ inside the heterojunction. To calculate the VBO as defined by $VBO \equiv E_v(A)' - E_v(B)'$, we start from the following relationship:

$$E_v(A) - E_{es}(A) = E_v(A)' - E_{es}(A)', \quad (5)$$

$$E_v(B) - E_{es}(B) = E_v(B)' - E_{es}(B)'. \quad (6)$$

The physical meaning of the above equations is that the difference between the energy edge and the average electrostatic potential of a bulk material keeps unchanged. We can easily obtain from the above equations as

follows:

$$E_v(A)' - E_v(B)' = [E_v(A) - E_{es}(A)] - [E_v(B) - E_{es}(B)] + [E_{es}(A)' - E_{es}(B)']. \quad (7)$$

The difference of the first two square brackets correspond to the energy difference ΔE_v of the valence band edges for the two bulk semiconductors A and B that form the heterojunction, and the items in the third square brackets give the lineup of the potential ΔV through the heterojunction. For the conduction band offset, the same calculation procedure can be applied. Therefore, the band offset can be calculated as [52–54]

$$VBO(CBO) = \Delta E_{v(c)} + \Delta V, \quad (8)$$

where $\Delta E_v(\Delta E_c)$ is defined as the difference between the top (bottom) of the valence (conduction) bands of the two independent bulk materials that form the heterojunction, ΔV is the lineup of the potential through the heterojunction. In this paper, to determine the band offset values of ZnO/BeCdO, a superlattice containing nine unit cells of pure ZnO and nine unit cells of $Be_{0.44}Cd_{0.56}O$ was used to calculate the potential profile through the heterojunction. The interface calculation is performed for a nonpolar $[1\,1\,\bar{2}\,0]$ surface. This is accomplished if a bulk-like region in the center of each layer can be identified, allowing for a proper determination of the average of the electrostatic potential far from the interface. The experimental lattice constants of hexagonal *wurtzite* ZnO [38], $a = 3.2495$ Å, $c/a = 1.602$, and $u = 0.382c$, were used in our calculations for pure ZnO and all the BeCdO alloys. A $12 \times 12 \times 2$ k-mesh were used to sample the Brillouin Zone of the heterojunctions.

Our calculated band offsets and the corresponding atomic structure of the heterojunction are shown in Figure 3, the band alignment of $ZnO/Be_{0.44}Cd_{0.56}O$ heterojunction is type II with CBO = 0.50 eV and VBO = 0.28 eV. We note that the CPA does not include local relaxations so that the interface stays rigid in our calculations. How the microscopic details affect the band offset still needs a further study. To understand why type II band offset in $ZnO/Be_{0.44}Cd_{0.56}O$ heterojunction was achieved, it must to recall the band alignment of ZnO/BeO heterojunction, in which the valence band maximum of BeO is of lower energy than that of ZnO, while the conduction band minimum of BeO is of higher energy than that of ZnO [55]. A type I energy alignment was formed. This is because the *p-d* (*p* orbital of O and *d* orbital of Zn) repulsion pushes up the valence band maximum, whereas Be have no active d electrons [51]. As Cd is doped in BeO, the valence band maxima of BeCdO shift upwards due to the repulsion effect between Cd-*4d* and O-*2p*, and with the increasing of Cd concentration in

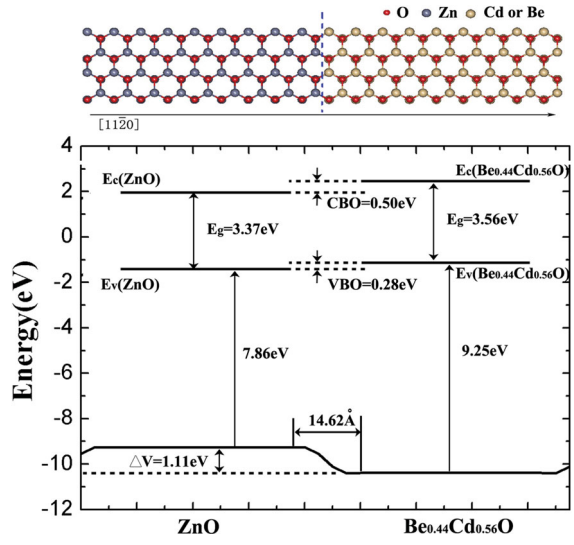

Figure 3. (Color online) Schematic plot of the calculated band alignment of $ZnO/Be_{0.44}Cd_{0.56}O$ heterojunction. A type II heterojunction is aligned in the staggered arrangement.

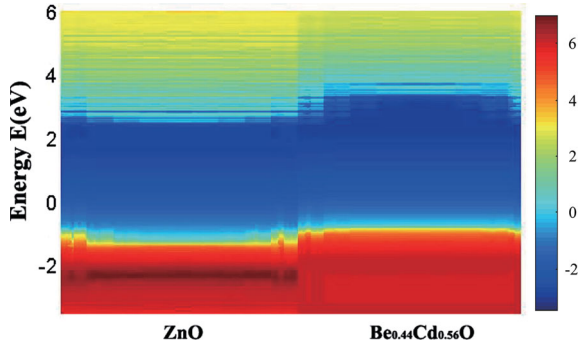

Figure 4. (Color online) Local projected density of states of $ZnO/Be_{0.44}Cd_{0.56}O$ heterojunction. The blue region indicates the band gap, and type II band alignment can be observed.

$Be_{1-x}Cd_xO$ alloy, the repulsion effect between Cd-*4d* and O-*2p* is enhanced. Especially, for x = 0.56, in our model the valence band maximum of $Be_{0.44}Cd_{0.56}O$ will higher than that of ZnO. As a result, a type II energy alignment was formed in $ZnO/Be_{0.44}Cd_{0.56}O$ heterojunction. From the analysis, we can find that the band offsets of the heterojunction are strongly dependent on Cd composition, just as reported in the ZnO/ZnCdO heterojunction [5].

Besides using the above calculation method to accurately determine the band offset values, a more intuitive way to obtain the band alignment is to calculate the local projected density of states (LPDOS) of the heterojunction [56–58], through which we can obtain the band alignment of the heterojunction directly, and an intrinsic staggered band offset (type II band alignment) can be observed as shown in Figure 4. Clearly, the LPDOS indicated band offsets qualitatively agree well with our accurately determined band offset values.

4. Summary

We have predicted the band gaps across the entire concentration range for $Be_{1-x}Cd_xO$ and band offset of *lattice matched* $ZnO/Be_{0.44}Cd_{0.56}O$ heterojunction using from first principles under LMTO scheme with CPA-MBJ approach. Our calculated results show that the heterojunction has a type II band alignment with the CBO and VBO being 0.50 and 0.28 eV, respectively. It can be expected that this approach can be used to predict more band information for semiconductor alloys and heterojunction.

Disclosure statement

No potential conflict of interest was reported by the authors.

Funding

This work was supported by the National Natural Science Foundation of China (grant nos. 11504072, 11774217 and 11404273).

ORCID

Yin Wang http://orcid.org/0000-0001-5500-1228

References

[1] Franciosi A, Van de Walle CG. Heterojunction band offset engineering . Surf Sci Rep. 1996;25:1–140.
[2] Li BW, Wang Y, Xie YQ, et al. Strain controlled switching effects in phosphorene and GeS. Nanotechnology. 2017;28:435202.
[3] Zeng YJ, Jian ZX, Ye ZZ, et al. Growth of Al–CN codoped p-type ZnMgO thin films on different substrates. Superlattices Microstruct. 2008;43:278–284.
[4] Zeng W, Yang X, Shang M, et al. Fabrication of Mg-doped ZnO nanofibers with high purities and tailored band gaps. Ceram Int. 2016;42:10021–10029.
[5] Yin HT, Chen J, Wang Y, et al. Composition dependent band offsets of ZnO and its ternary alloys. Sci Rep. 2017;7:41567.
[6] Su SC, Lu YM, Zhang ZZ, et al. Valence band offset of $ZnO/Zn_{0.85}Mg_{0.15}O$ heterojunction measured by X-ray photoelectron spectroscopy. Appl Phys Lett. 2008;93:082108.
[7] Reynolds DC, Look DC, Jogai B, et al. Valence-band ordering in ZnO. Phys Rev B. 1999;60:2340–2344.
[8] Huang MH, Mao S, Feick H, et al. Room-temperature ultraviolet nanowire nanolasers. Science. 2001;292:1897–1899.
[9] Mohseni H, Mensah BA, Gupta N, et al. Exceptional friction mitigation via subsurface plastic shear in defective nanocrystalline ceramics. Mater Res Lett. 2015;3:23–29.
[10] Nuruddin A, Abelson JR. Improved transparent conductive oxide/p+/i junction in amorphous silicon solar cells by tailored hydrogen flux during growth. Thin Solid Films. 2001;394:48–62.
[11] Nakahara K, Akasaka S, Yuji H, et al. Nitrogen doped $Mg_xZn_{1-x}O/ZnO$ single heterostructure ultraviolet light-emitting diodes on ZnO substrates. Appl Phys Lett. 2010;97:013501.
[12] Tang ZK, Wong GKL, Yu P, et al. Room-temperature ultraviolet laser emission from self-assembled ZnO microcrystallite thin films. Appl Phys Lett. 1998;72:3270–3272.
[13] Wang K, Chen J, Zhou W, et al. Direct growth of highly mismatched type II ZnO/ZnSe core/shell nanowire arrays on transparent conducting oxide substrates for solar cell applications. Adv Mater. 2008;20:3248–3253.
[14] Wang K, Chen JJ, Zeng ZM, et al. Synthesis and photovoltaic effect of vertically aligned ZnO/ZnS core/shell nanowire arrays. Appl Phys Lett. 2010;96:123105.
[15] Wang X, Zhu H, Xu Y, et al. Aligned ZnO/CdTe coreshell nanocable arrays on indium tin oxide: synthesis and photoelectrochemical properties. ACS Nano. 2010;4:3302–3308.
[16] Guo X, Zhu H, Li Q. Visible-light-driven photocatalytic properties of $ZnO/ZnFe_2O_4$ core/shell nanocable arrays. Appl Catal B. 2014;160–161:408–414.
[17] Ohtomo A, Tamura K, Saikusa K, et al. Single crystalline ZnO films grown on lattice-matched $ScAlMgO_4$(0 0 0 1) substrates. Appl Phys Lett. 1999;75:2635–2637.
[18] Srikant V, Speck J, Clarke DR. Mosaic structure in epitaxial thin films having large lattice mismatch. J Appl Phys. 1997;82:4286–4295.
[19] Almamun Ashrafi ABM, Binh NT, Zhang B, et al. Strain relaxation and its effect in exciton resonance energies of epitaxial ZnO layers grown on 6H-SiC substrates. Appl Phys Lett. 2004;84:2814–2816.
[20] Sun Y, Cherns D, Doherty RP, et al. Reduction of threading dislocations in ZnO/(0 0 0 1) sapphire film heterostructure by epitaxial lateral overgrowth of nanorods. J Appl Phys. 2008;104:023533.
[21] Van de Walle CG, Martin RM. Theoretical study of band offsets at semiconductor interfaces. Phys Rev B. 1987;35:8154–8165.
[22] Van de Walle CG, Neugebauer J. Universal alignment of hydrogen levels in semiconductors, insulators and solutions. Nature. 2003;423:626–628.
[23] Walsh A, Catlow CRA. Structure, stability and work functions of the low index surfaces of pure indium oxide and Sn-doped indium oxide (ITO) from density functional theory. J Mater Chem. 2010;20:10434–10444.
[24] Wei SH, Zunger A. Calculated natural band offsets of all II–VI and III–V semiconductors: chemical trends and the role of cation d orbitals. Appl Phys Lett. 1998;72:2011–2013.
[25] Northrup JE, Hybertsen MS, Louie SG. Theory of quasiparticle energies in alkali metals. Phys Rev Lett. 1987;59:819–822.
[26] Heyd J, Scuseria GE, Ernzerhof M. Hybrid functionals based on a screened Coulomb potential. J Chem Phys. 2003;118:8207–8215.
[27] Feng R, Kremer F, Sprouster DJ, et al. Enhanced electrical activation in in-implanted $Si_{0.35}Ge_{0.65}$ by C co-doping. Mater Res Lett. 2017;5:29–34.
[28] Taylor J, Guo H, Wang J. Ab initio modeling of open systems: charge transfer, electron conduction, and molecular switching of a C_{60} device. Phys Rev B. 2001;63:121104(R).
[29] Taylor J, Guo H, Wang J. Ab initio modeling of quantum transport properties of molecular electronic devices. Phys Rev B. 2001;63:245407.
[30] Wang Y, Zahid F, Zhu Y, et al. Band offset of GaAs/$Al_xGa_{1-x}As$ heterojunctions from atomistic first principles. Appl Phys Lett. 2013;102:132109.

[31] Tran F, Blaha P. Accurate band gaps of semiconductors and insulators with a semilocal exchange-correlation potential. Phys Rev Lett. 2009;102:226401.
[32] Wang Y, Hin H, Cao R, et al. Electronic structure of III–V zinc-blende semiconductors from first principles. Phys Rev B. 2013;87:235203.
[33] Zhu Y, Liu L, Guo H. Green's function theory for predicting device-to-device variability. Phys Rev B. 2013;88:085420.
[34] César M, Ke Y, Ji W, et al. Band gap of $In_xGa_{1-x}N$: a first principles analysis. Appl Phys Lett. 2011;98:202107.
[35] Zhu Z, Xiao J, Sun H, et al. Composition-dependent band gaps and indirect-direct band gap transitions of group-IV semiconductor alloys. Phys Chem Chem Phys. 2015;17:21605–21610.
[36] Kudrnovský J, Drchal V, Maek J. Canonical description of electron states in random alloys. Phys Rev B. 1987;35:2487–2489.
[37] Zhu Y, Liu L. Atomistic simulation of quantum transport in nanoelectronic devices. Singapore: World Scientific; 2016.
[38] Lide DR, editor. CRC handbook of chemistry and physics. 73rd ed. New York (NY): CRC Press; 1992.
[39] Kim WJ, Leem JH, Han MS, et al. Crystalline properties of wide band gap BeZnO films. J Appl Phys. 2006;99:096104.
[40] Guerrero-Moreno RJ, Takeuchi N. First principles calculations of the ground-state properties and structural phase transformation in CdO. Phys Rev B. 2002;66:205205.
[41] Denton AR, Ashcroft NW. Vegard's law. Phys Rev A. 1991;43:3161–3164.
[42] Detert DM, Lim SHM, Tom K, et al. Crystal structure and properties of $Cd_xZn_{1-x}O$ alloys across the full composition range. Appl Phys Lett. 2013;102:232103.
[43] Koller D, Tran F, Blaha P. Improving the modified Becke–Johnson exchange potential. Phys Rev B. 2012;85:155109.
[44] In calculations with MBJ, the c' parameters are: ZnO crystal, $c' = 1.13$ for the atoms and 1.75 for the vacancy spheres; BeO crystal, $c' = 1.15$ for the atoms and 1.84 for the vacancy spheres.
[45] Schleife A, Fuchs F, Furthmüller J, et al. First-principles study of ground- and excited-state properties of MgO, ZnO, and CdO polymorphs. Phys Rev B. 2006;73:245212.
[46] Sakong S, Gutjahr J, Kratzer P. Comparison of density functionals for nitrogen impurities in ZnO. J Chem Phys. 2013;138:234702.
[47] Baumeier B, Krüger P, Pollmann J. Atomic and electronic structure of BeO and the BeO(1 0 $\bar{1}$ 0) surface: an ab initio investigation. Phys Rev B. 2007;75:045323.
[48] Duman S, Sütlü A, Bağcl S, et al. Structural, elastic, electronic, and phonon properties of zinc-blende and wurtzite BeO. J Appl Phys. 2009;105:033719.
[49] Ryu Y, Lee TS, Lubguban JA, et al. Wide-band gap oxide alloy: BeZnO. Appl Phys Lett. 2006;88:052103.
[50] Janotti A, VandeWall CG. Absolute deformation potentials and band alignment of wurtzite ZnO, MgO, and CdO. Phys Rev B. 2007;75:121201.
[51] Zheng SW, Fan GH, He M, et al. Study on the electronic structures and energy band properties of Cd-doped wurtzite BeO. Acta Phys Sin. 2012;61:177102.
[52] Colombo L, Resta R, Baroni S. Valence-band offsets at strained Si/Ge interfaces. Phys Rev B. 1991;44:5572–5579.
[53] Peressi M, Binggeli N, Baldereschi A. Band engineering at interfaces: theory and numerical experiments. J Phys D: Appl Phys. 1998;31:1273.
[54] Junquera J, Zimmer M, Ordejón P, et al. First-principles calculation of the band offset at $BaO/BaTiO_3$ and $SrO/SrTiO_3$ interfaces. Phys Rev B. 2003;67:155327.
[55] Shi HL, Duan Y. Band-gap bowing and p-type doping of (Zn, Mg, Be)O wide-gap semiconductor alloys: a first-principles study. Eur Phys J B. 2008;66:439–444.
[56] Wang Y, Yu Z, Zahid F, et al. Direct tunneling through high-κ amorphous HfO_2: effects of chemical modification. J Appl Phys. 2014;116:023703.
[57] Gao G, Li Z, Chen M, et al. Effect of molybdenum disulfide nanoribbon on quantum transport of graphene. J Phys: Condens Matter. 2017;29:435001.
[58] Chen M, Yu Z, Wang Y, et al. Nonequilibrium spin injection in monolayer black phosphorus. Phys Chem Chem Phys. 2016;18:1601.